buildings

MDPI

Article

Effects of Biochar on the Properties of Alkali-Activated Materials Containing Construction and Demolition Waste

Andrea Saccani *, Luca Baldazzi and Stefania Manzi

Department of Civil, Chemical, Environmental and Materials Engineering, University of Bologna, 40131 Bologna, Italy; luca.baldazzi4@unibo.it (L.B.); stefania.manzi4@unibo.it (S.M.)
* Correspondence: andrea.saccani@unibo.it; Tel.: +39-051-2090343

Abstract

The effect of biochar in metakaolin alkali-activated materials (AAMs) modified with construction and demolition waste (CDW) is analyzed to investigate mechanical properties and provide a preliminary assessment of durability. A 30 wt% mix of brick and concrete powders replaced metakaolin. At the same time, biochar replaced metakaolin in different amounts, ranging from 0.5 to 5.0 wt%. The results show that, in samples containing CDW, a further replacement of metakaolin with biochar up to 1 wt% increases the compressive strength, both at short curing times (+20% after 7 days) and longer curing (+30% after 28 days) when compared to the CDW-modified sample without biochar. The dimensional stability of CDW-modified samples increases, and biochar addition provides a further benefit. Moreover, biochar addition below 1.5 wt% also reduces water absorption by capillary. Both features could forecast improved durability of the biochar-modified materials, to be validated with long-term experiments.

Keywords: biochar; alkali-activated materials; construction and demolition waste (CDW); eco-friendly materials; capillary water absorption; dimensional stability

1. Introduction

Biochar is a solid product of the pyrolysis of organic material at high temperatures. Different production processes can be used, such as flash carbonization, microwave-assisted carbonation and steam gasification [1,2]. Due to the production processes, biochar contains a high amount of carbon (60–90 wt%). The physical, chemical, and micro-structural properties of biochar depend on the original matter, its dimensions and the process parameters [3]. After its obtainment, biochar can be subjected to various activation treatments to increase total porosity, specific surface area (≈1500 m^2/g), surface reactivity and adsorption capacity [3,4]. The biochar market is currently growing rapidly (+13.4%), particularly in the Asia–Pacific region, and it was evaluated at $1.8 billion globally in 2022, with a potential expected growth to $16 billion in 2028 [3]. At present, biochar is mainly used for soil remediation and as a soil amendment to improve the quality of agricultural lands. However, recent studies have also investigated its incorporation into traditional cement-based composites owing to its capability to capture atmospheric CO_2, thus acting as an eco-friendly adsorbent material. In particular, it was observed that the addition of less than 1% of biochar by weight in concrete will prevent the emission of around 0.5 Gt CO_2/year, that is, 20% of the yearly total emissions of CO_2 originating from the cement industry [1]. The replacement of ordinary Portland cement (OPC) mortar with 30% biochar as a fine aggregate and 9% metakaolin as a binder could sequester 59 kg CO_2/t, generating a potential profit of

Check for updates

Academic Editor: Piti Sukontasukkul

Received: 15 September 2026
Revised: 16 October 2026
Accepted: 21 October 2026
Published: 26 October 2026

Copyright: © 2026 by the authors. Licensee MDPI, Basel, Switzerland. This article is an open access article distributed under the terms and conditions of the Creative Commons Attribution (CC BY) license.

35.4 $/m^3 [5]. Another effect of adding biochar to OPC concrete is improvements in the compressive strength (+9% [6]; +5% [7]) for a replacement percentage near 1% of the fine aggregate. Chen [5] obtained a higher increment of strength (+20%) with the addition of 3% biochar pyrolyzed at 500 °C coming from corn straw.

This improvement is connected to the filler effect leading to better packing and a denser matrix and to the water retention capacity of biochar [8]. The filler effect of inert carbon particles can be more efficient in cement paste than the pozzolanic reaction [5]. A second reason for the increase in strength is that biochar can absorb part of the free water in the paste, thereby reducing the effective water–binder ratio. The water retained by the biochar is subsequently released gradually, supporting further cement hydration [5]. The addition of pre-saturated biochar (2% by weight of cement) reduces the autogenous shrinkage of concrete (−10%) by mitigating self-desiccation [9]. The presence of biochar decreases water penetration and sorptivity in traditional cement mortar owing to its high impermeability and small particle size, which promotes a microfiller effect [10]. Regarding fresh-state properties, the porous nature and low density of biochar reduce both the fresh density and workability of the mixture [10]. As the need to reduce polluting emissions becomes increasingly urgent, new materials, such as alkali-activated materials and geopolymers, have been tested as alternatives to traditional ordinary Portland cement [11]. The incorporation of biochar into these composites has not been extensively investigated, and its effects seem to be rather complex. This may arise from variations in the chemical structure of biochar depending on its source, as well as from its microstructure, which comprises different pore size fractions. These features are influenced by both the feedstock and the thermal treatment, as previously underlined. In particular, the surface of biochar has many functional groups and chemically reactive sites that can interact either with reactive powders such as fly ash [12] or with the active components of the alkali-activated materials, thereby affecting fresh-state rheology, promoting the formation of stable phases, and influencing gel formation. The porous nature of biochar tends to increase the overall porosity of the material, potentially leading to stress concentration and reduced mechanical properties [13,14] unless specific treatments are applied [12,15]. However, owing to its high specific surface area, biochar acts as a nucleation site for the formation of reaction products. Indeed, pastes containing small amounts of biochar (<2 wt%) have shown slightly higher compressive strength than the reference sample [13,16]. Moreover, biochar reduces autogenous shrinkage through internal curing provided by the release of previously absorbed water. This increases the relative humidity within the pore structure and decreases the capillary forces responsible for autogenous shrinkage [13].

On the other hand, the generation of construction and demolition waste is steadily increasing worldwide. The USA generated approximately 600 million tons of CDW in 2023, Canada 3.2 million tons in 2016, Australia 20.4 million tons in 2016–2017, and the European Union 337 million tons in 2014. China generates 2360 million tons annually, while Mexico and Brazil generate 12 and 45.1 million tons each year, respectively [17]. CDW disposal is becoming a growing concern from both an environmental and an economic perspective, as most of these materials are sent to landfill and disposal costs continue to rise. The possibility of reusing CDW in the production of new recycled concrete can generate savings by reducing costs and CO_2 emissions. However, to obtain mechanical strength comparable to that of the unmodified composites, the CDW replacement rate should be limited, in many cases to no more than 30%. The greatest cost-effectiveness and CO_2 emission reductions are achieved by using 10% recycled concrete powder and 20% recycled brick powder as replacements [18]. Moreover, CDWs have been investigated as potential precursors for the production of alkali-activated materials owing to their chemical composition, which is rich in Al and Si [19–23].

In this research, a preliminary investigation into the effects of biochar on CDW-modified alkali-activated materials is performed. Indeed, the positive effect of adding small amounts of biochar to metakaolin-based composites has already been demonstrated by the authors [16]. To further enhance the environmental benefits, it is of interest to evaluate the combined use of both materials (CDW and biochar), an approach that has not been extensively investigated in the literature. The incorporation of biochar could also counteract the reduction in mechanical properties resulting from the addition of CDW. A lack of understanding of the effects of biochar on the physical, mechanical and durability properties hinders the use of this material in construction applications. The investigated systems are rather complex since the actual reactivity of the different types of CDW is not precisely known. The research is thus confined to one percentage of CDW addition (30 wt%) and one ratio (1:1 wt% ratio) of concrete and brick amounts. On account of the variability of biochar composition, functionalities and particle size, the results will strictly pertain to the present conditions but can still outline a general trend.

2. Materials and Methods

2.1. Materials

2.1.1. Binders

Metakaolin. Argicem metakaolin, hereafter referred to as MTK, supplied by Argeco Développement (Fumel, France), was used to prepare the pastes. It is obtained by rapid calcination of a kaolinitic clay using a process developed by Argeco that ensures low energy consumption and low CO_2 emissions.

Concrete waste. The concrete waste used in this study comes from the demolition of the load-bearing structure of "Punta Perotti" building complex that took place in 2006 in Bari (Italy). Since only the structural frame had been completed at the time of the demolition, this CDW consists entirely of crushed concrete [24,25]. Concrete chunks were ground using a laboratory jar mill (MMS, Nonantola, Modena, Italy) to obtain a very fine powder (<0.075 mm).

Brick waste. Brick waste was obtained from the demolition of a 19th-century building in Bologna (Italy). Bricks were ground using the same procedure as the concrete chunks.

Biochar. Biochar was kindly provided by Sorrenti [26]. This biochar is produced by Romagna Carbone snc, located in Bagnacavallo (Ravenna, Italy), and it is derived mainly from chipped peach and grapevine wood subjected to slow pyrolysis at temperatures up to 500 °C. Since the as-received biochar had a non-homogeneous particle size distribution and contained coarse particles, it was manually ground using a brass mortar and passed through a 0.50 mm sieve. The specific surface area of biochar measured with BET analysis (Nova 800, Anton Paar, Graz, Austria) is 10.48 m^2/g. A pH value of 9.97 is reported in [26].

All the powders were analyzed by X-ray diffraction using an Empyrean diffractometer (Malvern Panalytical, Almelo, The Netherlands), equipped with a PIXcel1D detector, and a Cu radiation source operated at 40 kV and 20 mA. Measurements were performed over a 2θ range of 4–100°, with a step size of 0.026° and a measurement time of 246.84 s per step. The software used for phase identification was High Score. The diffractograms are shown in Figure 1.

The XRD pattern of biochar reveals the peak of carbon at 26.5°. The presence of peaks around 25° indicates crystalized materials that have not yet reached a fully developed crystalline structure. Pyrolysis at high temperatures promotes the formation of microcrystalline carbon structures. The loss of crystallinity in cellulose is underlined by the presence of a broad peak around 20–24°. The increase in the intensity of the peak at 43.7° can be attributed to disordered carbonaceous structures. The lack of a peak at 14.9° indicates that cellulose decomposed almost completely at high temperature. Calcium carbonate

and quartz are inorganic phases also present in biochar. The XRD pattern of brick waste detected the presence of quartz as the main mineral phase. Muscovite, albite, iron oxide and anorthite were also detected. In concrete waste, only calcium carbonate peaks were detected. Metakaolin contains quartz and residuals of unreacted kaolinite.

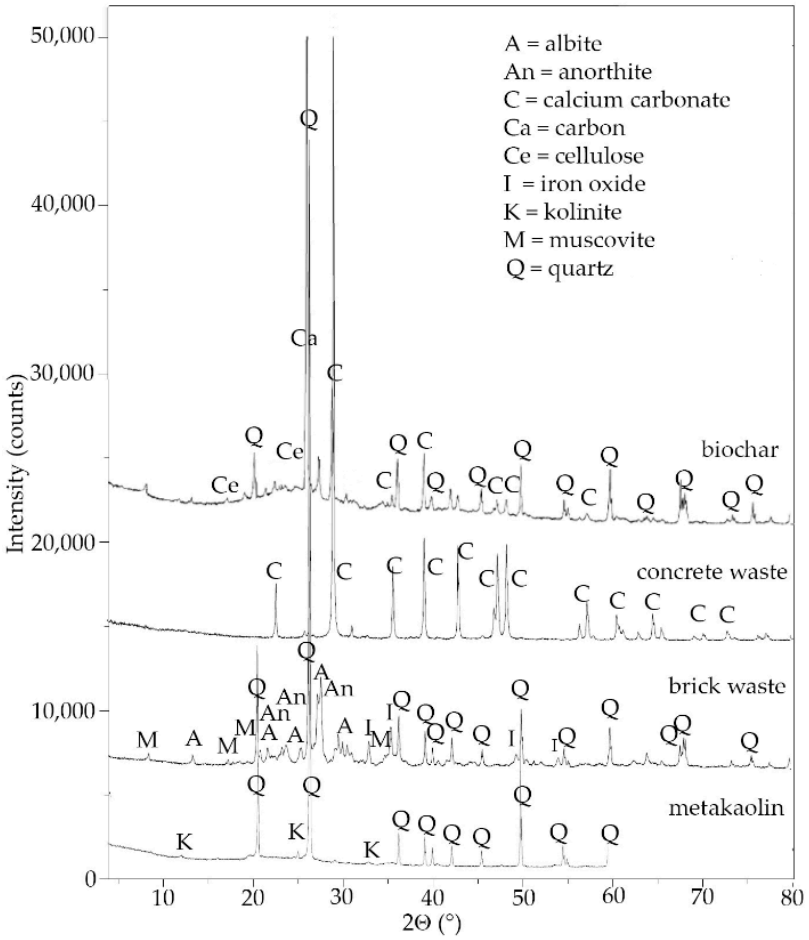


Figure 1. XRD of the investigated powders.

Thermogravimetric analysis (TGA 55, TA Instruments, Waters LLC, New Castel, DE, USA) was performed on the constituents. Tests were performed by analyzing the weight loss on platinum holders of 25 ± 3 mg of constituents at a ramp speed equal to 15 °C·min^{-1} from 30 °C to 950 °C in a 40 mL/min nitrogen flow (Figure 2). The thermograms show an initial weight decrease (10%) in biochar linked to humidity loss. Afterwards, a further drop takes place till 500 °C (15%), underlying an incomplete degradation of cellulose during pyrolysis, followed by a constant weight loss until the highest temperature is reached, leading to the formation of a complex char structure. The pulverized concrete sample shows two loss peaks related to the presence of C-S-H (near 450 °C) and calcium carbonate (range 700–800 °C). Brick waste powders are substantially inert.

The chemical composition of the constituents was obtained using EDAX analysis in a scanning electron microscope SEM XL20 type applying a voltage of 20 kV (FEI Instruments, FEI, Hillsboro, OR, USA). The weight in percentage of the elements detected is reported in Table 1.

The density of the powders was measured using a helium pycnometer (Ultrapycnometer 1000, Quantachrome Instruments, Boynton Beach, FL, USA) and the results are reported in Table 2. While the inorganic powders have similar values, biochar discloses a lower density value owing to its organic nature.

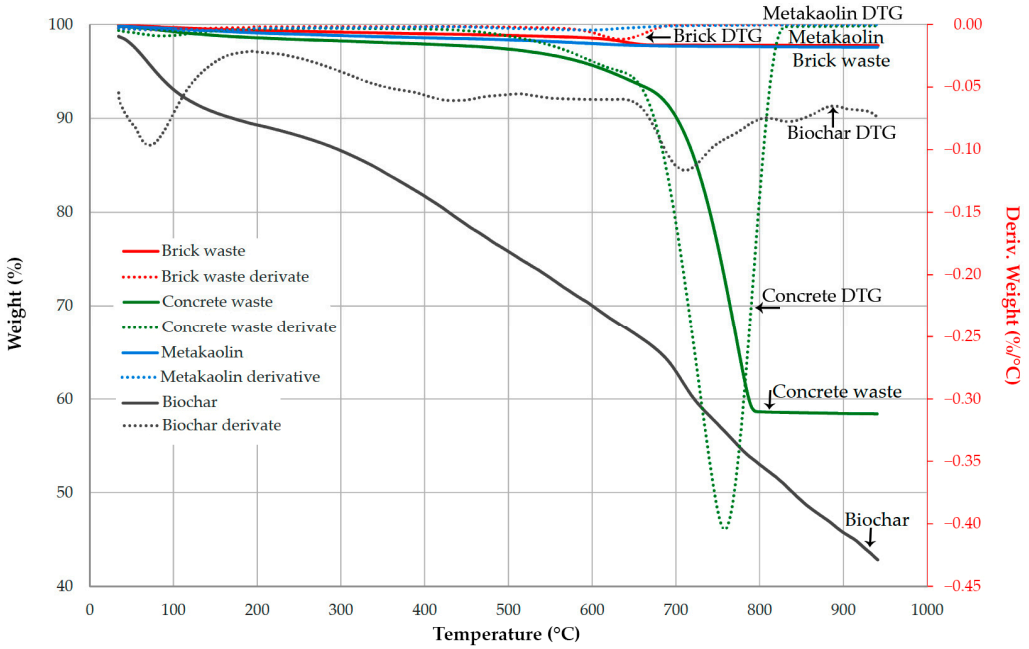


Figure 2. TGA graphics of the investigated powders.

Table 1. Weight percentage (%) of the elements detected in the constituents.

	C	O	Na	Mg	Al	Si	K	S	Ca	Ti	Fe
MTK	0.00	49.40	0.00	0.00	11.70	33.60	0.10	0.00	0.80	1.20	1.40
Concrete waste	7.50	22.80	0.00	0.99	0.77	3.34	0.00	0.62	59.85	0.00	4.20
Brick waste	0.00	23.29	1.51	2.26	9.60	34.50	3.50	0.00	8.52	0.00	11.50
Biochar	86.55	8.45	0.11	0.35	0.73	1.80	0.30	0.00	0.29	0.00	0.00

Table 2. Density of the constituents measured with helium pycnometer (g/cm^3).

MTK	Concrete Waste	Brick Waste	Biochar
2.627	2.741	2.865	1.961

2.1.2. Activators

NaOH solution. To activate the metakaolin and the concrete/brick powders, an 8 M solution of NaOH (Merck, Darmstadt, Germany) was previously prepared.

Sodium silicate. A commercial Na_2SiO_3 solution, designated as Reoflux B (SS, Ingessil, Verona, Italy) and characterized by a H_2O content of 56 wt%, a SiO_2/Na_2O ratio of 2.07 and a density of 1.53 g/cm^3, was also used as an activator.

The activators were previously mixed and cooled at room temperature before mixing with the powders.

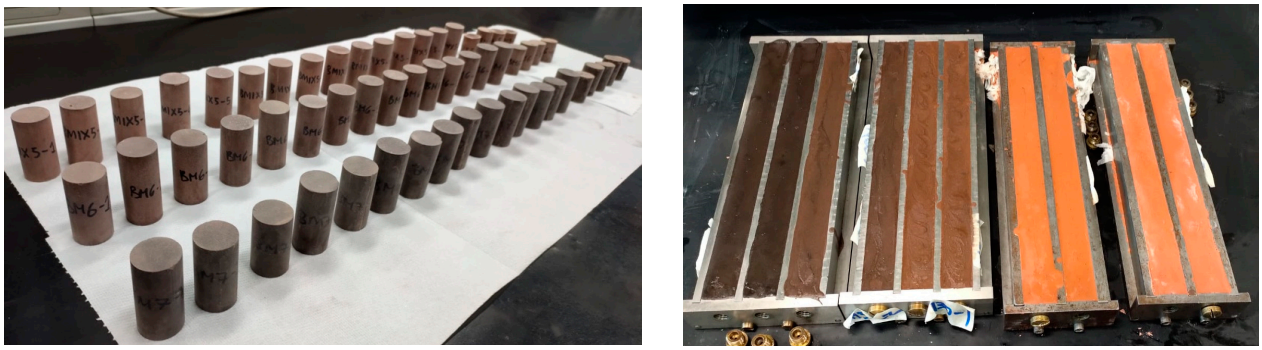
2.2. Mix Design and Sample Preparation

The formulated recipes of the alkali-activated binders with metakaolin, concrete and bricks wastes, and biochar are reported in Table 3. A first reference sample, named M-0, was prepared with 100 wt% of metakaolin. Then, the mix M30-0 was created by substituting 30 wt% of MTK with a mix made up of 50 wt% concrete waste and 50 wt% brick waste (CDW) according to other studies [27]. Starting from this mix design, the metakaolin was substituted with the following amounts of biochar in an air-conditioned state: 0.5 wt%, 1 wt%, 1.5 wt%, 2 wt%, 3.5 wt% and 5 wt% (M30-0.5, M30-1, M30-1.5, M30-2, M30-3.5 and M30-5). The binder/activator ratio was kept constant, equal to 1.32, although this caused

a progressive misbalance in the Si/Al and Na/Al ratio due to the different composition of the powders, particularly above 2%. The two activators were used in the same amount (NaOH solution: sodium silicate = 1:1). The pastes were prepared using a beaker (1 L volume) and a mixer (Janke & Kunkel IKA, Labortechnik RW-20, Haverhill, MA, USA). Initially, all the powders (metakaolin, biochar, concrete and brick waste) were weighed and placed in the beaker. The previously mixed and cooled activation solution (NaOH and Na_2SiO_3) was added in a continuous flux during the first minutes of the mixing process. After 4 min and 30 s of mixing at medium speed, the mixer was stopped for 30 s. An additional mixing of 30 s at high speed followed to obtain a homogeneous paste, for a total mixing time of 5 min. For each recipe, 27 cylindrical samples (ϕ 27 mm × height 55 mm) and 3 prismatic samples (25 × 25 × 285 mm) with a gauge length of 250 mm were prepared (Figure 3). The former were used for physical (bulk density, water absorption by capillary test, water absorption, and open porosity) and mechanical tests (compressive strength (at 7, 14, 28 days) and dynamic elastic modulus). The prismatic samples were used for length change determination. After 24 h in sealed polyethylene bags, all samples were demolded. All cylinders were consequently stored in polypropylene boxes with hermetic cover at laboratory temperature (22 ± 1 °C, 60 ± 10 RH%). The prismatic samples were placed in a climatic chamber (DY430, Angelantoni, Massa Martana, Italy) at 30 °C and 40% RH until measurement.

Table 3. Binder amounts of the investigated mixes expressed in weight percentage.

Sample	MTK	Concrete Waste	Brick Waste	Biochar
M-0	100.00	0.00	0.00	0.00
M30-0	70.00	15.00	15.00	0.00
M30-0.5	69.50	15.00	15.00	0.50
M30-1	69.00	15.00	15.00	1.00
M30-1.5	68.50	15.00	15.00	1.50
M30-2	68.00	15.00	15.00	2.00
M30-3.5	66.50	15.00	15.00	3.50
M30-5	65.00	15.00	15.00	5.00



(**a**) (**b**)

Figure 3. Cylindrical (ϕ 27 mm × height 55 mm) (**a**) and prismatic (25 × 25 × 285 mm) (**b**) alkali-activated samples.

2.3. Methods

2.3.1. Determination of Standard Consistency

Standard consistency was determined using a brass truncated conical mold (ϕ 20–40 mm, 60 mm height). Immediately after the end of the mixing, the paste was poured inside the mold up to the top, and the potential surplus was removed. After the removal of the mold,

two perpendicular diameters of the collapsed paste were measured. Standard consistency (C) was then calculated using Equation (1):

$$C = 100 \cdot (d_m - d_0)/d_0, \quad (1)$$

where d_m is the average diameter of the two perpendicular diameters and d_0 is the lower diameter of the mold (i.e., 40 mm).

2.3.2. Physical Properties

The bulk density (ρ_b), water absorption (WA) at atmospheric pressure and total open porosity (OP) of the alkali-activated pastes were performed after 28 days of curing at room temperature, according to the EN 772-13 [28], and EN 772-21 [29] Standards, respectively. Specimens were weighted in dry, wet, and hydrostatic conditions. Initially, three cylinders for each recipe were dried in an oven at 40 °C for 48 h. A lower temperature (40 instead of 70 °C) was chosen in order to prevent as much as possible further reactions inside the materials. Samples were then measured to obtain the dry weight. Later, the cylinders were submerged in distilled water in polypropylene boxes with hermetic cover. After approximately 48 h, the samples were measured in hydrostatic condition and wet condition (saturated dry surface condition obtained with a wet towel). After two measurements (48 h and 72 h) with a difference lower than 0.2%, the final weight in wet and hydrostatic conditions was recorded.

After 28 days of curing at room temperature, other three cylinders were used to measure the water absorption by capillary, according to EN 15801 [30]. The amount of water absorbed was calculated using Equation (2):

$$Q_i = (m_i - m_0)/A, \quad (2)$$

where Q_i is the amount of absorbed water at time t_i (kg/m^2), m_i is the weight of the sample at time t_i (kg), m_0 is the weight of the dried sample (kg), and A is the absorption area in contact with water (m^2).

2.3.3. Mechanical Properties

Compressive strength (σ_c) was determined using a 100 kN Wolpert testing machine (Wolpert, Neu Ulm, Germany) at a displacement rate of 5 mm/min. Six cylindrical specimens (ϕ 27 mm $\times$ height 55 mm) from each series were tested after 7, 14 and 28 days of curing at 22 $\pm$ 1 °C and relative humidity of 60 $\pm$ 10%. After 28 days of curing, the dynamic elastic modulus (E_d) was also measured using an ultrasonic pulse velocity tester (Matest C369N, Treviolo, BG, Italy), in accordance with EN 12504-4 [31], using Equation (3):

$$E_d = V^2 \cdot \rho \cdot (1 + \nu) \cdot (1 - 2\nu)/(1 - \nu), \quad (3)$$

where E_d is the dynamic elastic modulus (Pa), V is the pulse velocity (m/s), ρ is the density of the sample (kg/m^3) and ν is Poisson's ratio considered equal to 0.25, according to Yan's research on metakaolin based pastes [32], and thus assuming a negligible effect of biochar to be further confirmed.

2.3.4. Microstructure

Fragments of broken samples of alkali-activated pastes were collected after the compression test, performed after 28 days of curing, and observed with a scanning electron microscope SEM XL20 type applying a voltage of 20 kV (FEI Instruments, FEI, Hillsboro, OR, USA), equipped with an energy dispersive spectroscopy (EDS) X-ray detector. The fractured surfaces of the samples were coated with graphite to ensure electrical conductivity.

2.3.5. X-Ray Diffraction Analysis and Thermogravimetric Analysis

A part of the smaller fragments of the cylinders, broken during the compression test after 28 days of curing, were collected and ground with an agate mortar to obtain a very fine powder (<75 μm). The powder was used to perform X-ray diffraction analysis and later thermogravimetric analysis with the instruments and procedure described before.

2.3.6. Dimensional Stability

The length at time x (L_x) of the three prismatic samples was measured using a length comparator previously calibrated using a reference steel bar. The change in length at x age (L) was evaluated in accordance with the ASTM C 490/C 490M–08 Standard [33], using Equation (4):

$$L = (L_x - L_i) \cdot 100/G, \quad (4)$$

where L_x is the comparator reading of the specimen at x age minus the comparator reading of the reference bar at x age (mm), L_i is the initial comparator reading of the specimen minus the initial comparator reading of the reference bar at that same time (mm), and G is the nominal gauge length (250 mm).

3. Results and Discussion

Table 4 reports the standard consistency results, namely, the average diameter (d_m) and final consistency (C), together with bulk density (ρ_b). Water absorption (WA) and open porosity (OP) are presented graphically in Figure 4. Comparing reference samples (i.e., M-0 and M30-0), it can be observed that replacing metakaolin with brick and concrete wastes creates more workable pastes. The M-0 sample shows the lowest workability. The consistency of the samples also decreases with the replacement of biochar. The effect is mainly caused by biochar porosity, since it absorbs water from the pastes, creating higher viscosity. A contribution can also derive from biochar morphology and interparticle interactions. Concerning water absorption (WA), the results are substantially similar in all samples (ranging from 21.9 to 23.4%). Nevertheless, a steady and almost linear increase in WA takes place as the amount of biochar increases. Similar observations can be made for open porosity (OP), although a more complex trend is observed.

Table 4. Consistency and bulk density (and relative standard deviation) of investigated pastes.

Sample Name	% Biochar	dm (mm)	C (%)	ρb (g/cm3)
M-0	0	118	195	1.50 ± 0.02
M30-0	0	143	258	1.51 ± 0.01
M30-0.5	0.5	140	250	1.49 ± 0.01
M30-1	1	135	238	1.49 ± 0.01
M30-1.5	1.5	134	235	1.48 ± 0.02
M30-2	2	133	233	1.48 ± 0.01
M30-3.5	3.5	125	213	1.47 ± 0.01
M30-5	5	120	200	1.45 ± 0.01

d_m = average diameter measured during the standard consistency test; C = consistency; ρ_b = bulk density.

The compressive strength (σ_c) of all the samples after 7, 14 and 28 days of curing is reported in Table 5, along with the corresponding standard deviations. For clarity and ease of comparison, the results are also presented graphically in Figure 5.

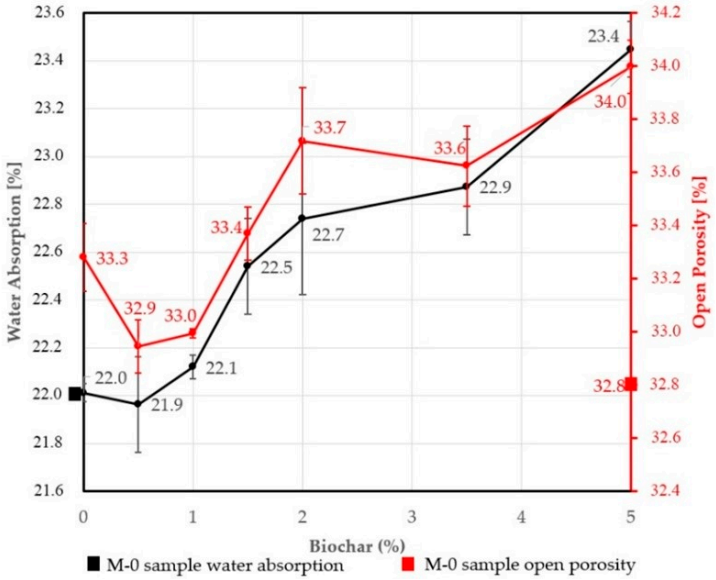


Figure 4. Water absorption (black) and open porosity (red) curves of alkali-activated materials (single square signs refer to reference sample M-0). Standard deviation is reported (three specimens).

Table 5. Compressive strength (σ_c) and standard deviation of investigated pastes after 7, 14 and 28 days of curing.

Sample Name	% Biochar	σ_c 7 Days (MPa)	σ_c 14 Days (MPa)	σ_c 28 Days (MPa)
M-0	0	20.5 ± 0.4	23.0 ± 2.1	28.5 ± 2.5
M30-0	0	20.0 ± 2.8	20.3 ± 0.3	25.5 ± 3.1
M30-0.5	0.5	21.3 ± 2.5	23.7 ± 4.0	28.3 ± 3.1
M30-1	1	24.0 ± 2.9	24.8 ± 2.3	33.2 ± 3.0
M30-1.5	1.5	21.5 ± 2.1	23.6 ± 4.0	27.8 ± 3.4
M30-2	2	21.3 ± 2.1	22.1 ± 2.0	25.2 ± 1.8
M30-3.5	3.5	20.0 ± 0.8	22.5 ± 1.1	25.0 ± 2.8
M30-5	5	18.7 ± 1.2	19.5 ± 3.1	25.7 ± 2.1

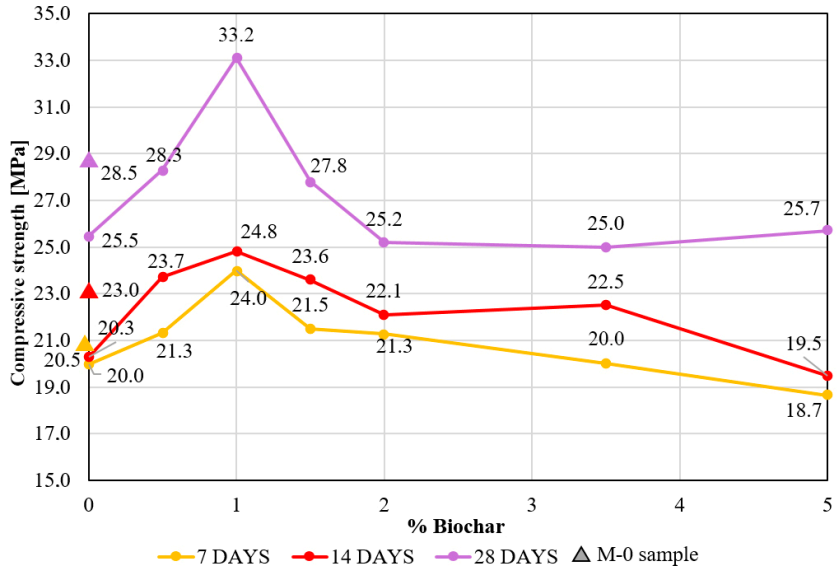


Figure 5. Compressive strength as a function of biochar content across different curing ages (triangle signs refer to unmodified metakaolin paste M-0). Data are the average of six specimens.

The M-0 sample shows slightly higher compressive strength than the M30-0 one, on account of the unbalanced ratios among the elements. Despite the higher porosity and possibly a lower interfacial bonding to the inorganic matrix of the biochar powders [12], a peak in strength is detected in the M30 samples at all curing times for a biochar addition equal to 1% (about +20% after 7 and 14 days, +30% after 28 days). The replacement of slightly higher amounts (between 1.5 and 2.0%) of biochar allows the mechanical loss caused by CDW addition to be almost completely balanced out. A further increase in biochar leads to comparable values of biochar-modified samples and M30-0. The compressive strength data of the M30-0 and M30-1 series after 28 days of curing were statistically analyzed with ANOVA, considering statistically distinguishable groups with *p*-values less than 0.05. Welch's one-way ANOVA indicated a statistically significant difference between the two groups, $F(1, 9.99) = 19.0$, $p = 0.001$. M30-1 exhibited a higher mean compressive strength than M30-0, with an increase of approximately 30%, as previously underlined.

The positive effect observed in compressive strength is also present in the dynamic elastic modulus after 28 days of curing (Figure 6). The M30-1 sample shows a slight increase in the dynamic elastic modulus (9.0 GPa compared with the reference sample 8.7 GPa) that, however, remains below the M-0 sample. At higher content, the organic nature of biochar has a negative effect on the dynamic elastic modulus.

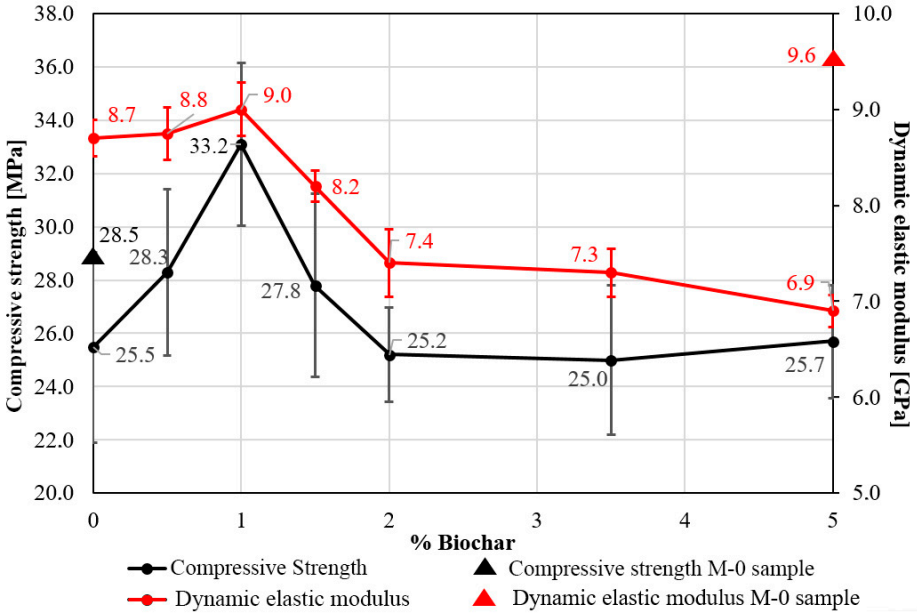


Figure 6. Compressive strength (black) and dynamic elastic modulus (red) after 28 days (triangle signs refer to unmodified metakaolin paste M-0). Standard deviation reported (six specimens).

Preliminary SEM observations disclose a dense microstructure in all the composites (Figure 7a–c), underlying an efficient, homogeneous dispersion of biochar particles without the formation of any clusters. No remarkable discontinuities in the biochar–matrix ITZ are detected at the investigated magnification, supporting the moderate increase in open porosity (Figure 4). A deeper investigation at higher magnification will be needed to underline the detailed structure and chemical composition at the ITZ. Small acicular crystals are also observed (Figure 7d) at the higher biochar content. This phase is probably composed of sodium carbonate formed due to the unbalance between reactive silicium and aluminum oxides and activators, fostered by an increased CO_2 permeability induced by biochar. These observations must be confirmed by further investigations.

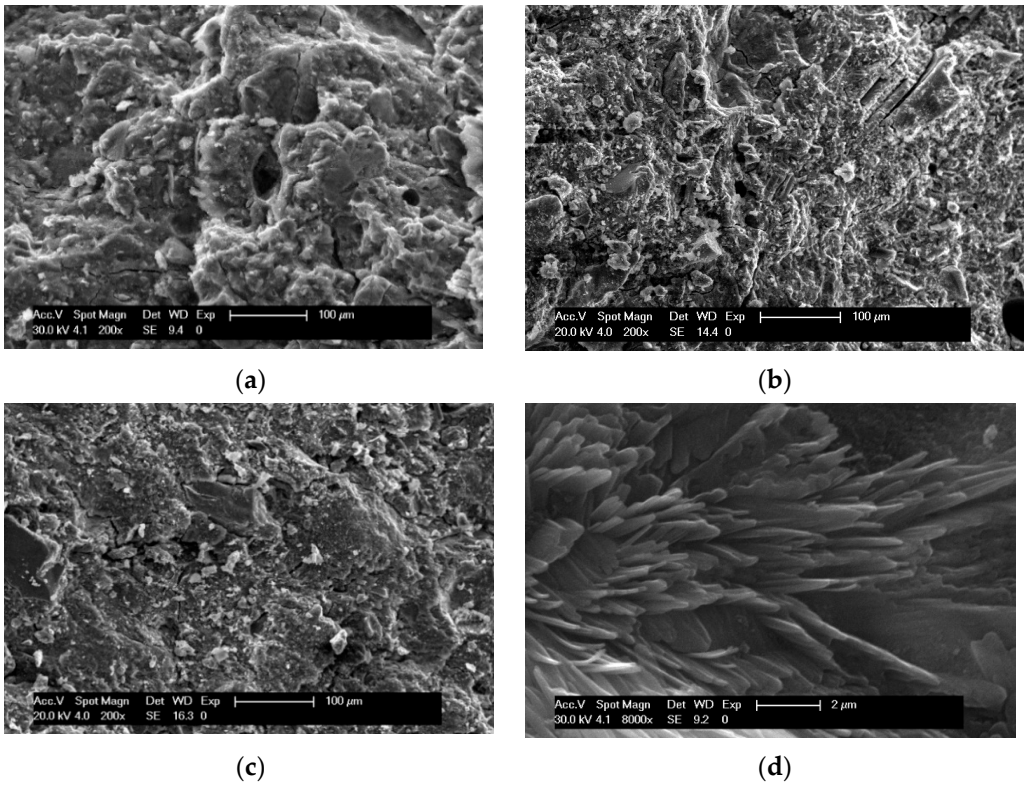


Figure 7. Microstructure of samples M30-0 (**a**), M30-1 (**b**), and M30-3.5 (**c**) and acicular crystals in M30-3.5 at higher magnification (**d**).

Figure 8 shows the XRD patterns of some of the most significant investigated samples. Quartz (Q) is the main phase detected in all the samples. Calcite (C, calcium carbonate), present in all the CDW modified samples (M30 series), derives from the concrete fraction and is consequently not present in the M-0 sample. The formation of sodium calcium aluminum silicate hydrate (N-C-A-S-H, Reference code 00-012-0228) possibly derives from the precursor effect of brick and concrete waste since during alkaline activation, concrete and brick waste (rich in SiO_2 and CaO) will promote the formation of these phases [34].

The TGA curves of the samples are shown in Figure 9. The percentage of losses in different ranges of temperature are reported in Table 6, corrected according to the water loss of biochar (Figure 2). The highest percentage of mass loss occurs in the range from 50 to 200 °C. This loss is due to the evaporation of the free water, adsorbed water and bound water from the alkaline gel [34,35]. The peak near to 120 °C can possibly be assigned to the dehydration of different types of calcium aluminum silicate hydrate such as C-(A)-S-H, C–(N)–A–S–H and C–S–H. Mass loss above 400 °C is probably related to the dehydration of the C–S–H. Peaks observed in the range 650–670 °C are all assigned to calcium carbonates with different crystallinity levels that belong mainly to concrete waste [34,35]. The slight hump pointed out near 540–570 °C at the higher biochar contents (5 and 2%) derives from the water loss of biochar. The total weight loss of the samples is minimum in M-0 samples, increasing in M30 samples, on account of the presence of calcium carbonate, and also slightly increasing with increasing biochar amount. The values are close to those found by Wichmann [34]. The low value of mechanical strength relative to sample M30-5 is reflected in the TGA analysis by the highest values of weight loss (about 22%). This can possibly be associated with the presence of a higher amount of loosely bound water in the network caused by the low degree of geopolymerization [36].

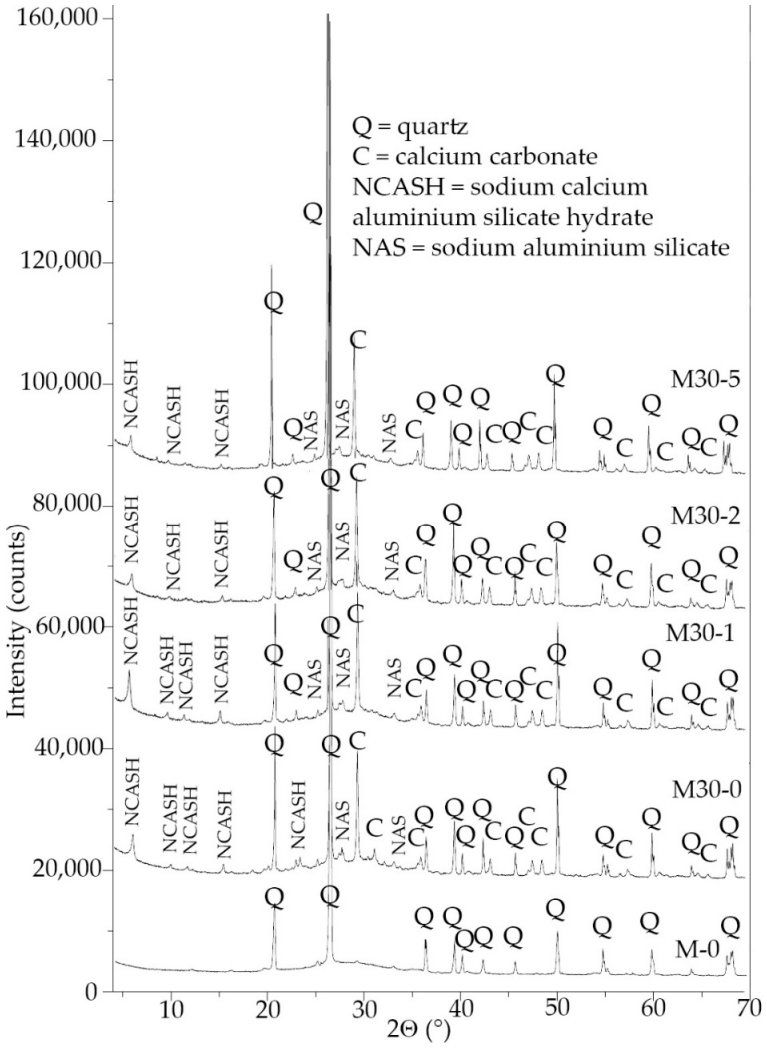


Figure 8. XRD diffractograms.

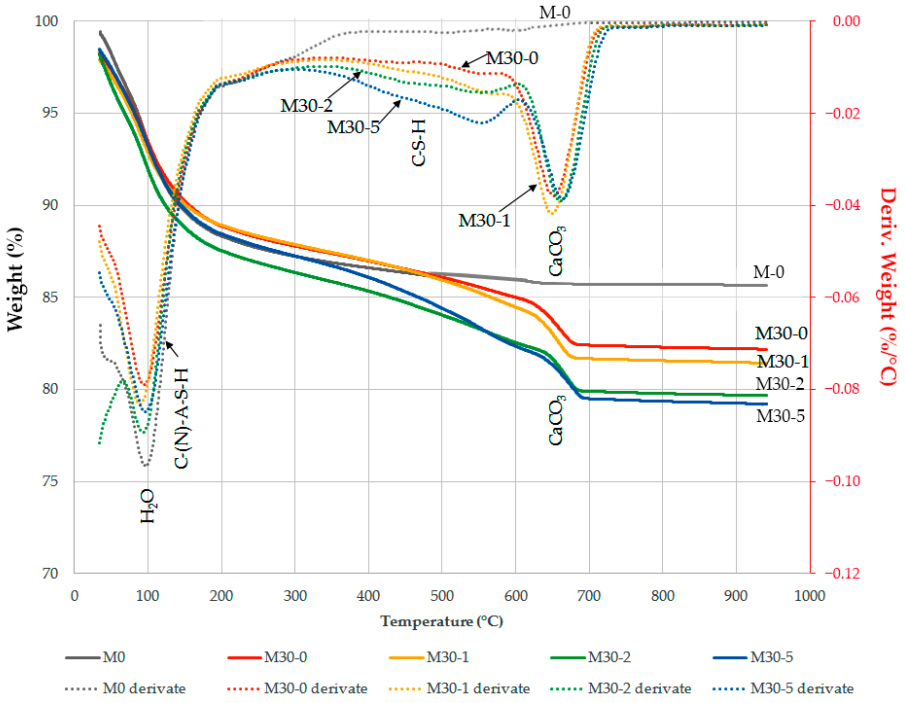


Figure 9. TGA results.

Table 6. Weight loss in percentage (%) of the samples during the TGA test.

Sample Name	0–200 °C	300–510 °C	610–710 °C
	H_2O + C-N-A-S-H	C-S-H	$CaCO_3$
M-0	12.2	0.0	0.0
M30-0	11.3	2.9	2.5
M30-1	11.2	3.0	2.6
M30-2	12.3	3.4	2.4
M30-5	11.3	3.7	2.3

In Figure 10, the water capillary absorption curves for all the samples are reported. The addition of CDW increases the rate of absorption when compared to the M0 sample, while the replacement of small amounts of biochar (<1.5%) generates the lowest ratios. At higher biochar amounts, no clear trend can be observed but the rates of absorption are even higher than that of M-0. The coefficient of capillary absorption discloses a decreasing trend from 0.1282 Kg/(m^2*$s^{0.5}$) for the M30-0 sample to 0.0826 for M30-0.5 and 0.0726 for M30-1.0. This behavior arises from a trade-off between the lower water affinity of biochar, prevailing at low amounts, and the increase in porosity (refer to Figure 4), also connected to the lower mechanical properties of CDW samples (M30 series) (Table 5). At high biochar contents, the negative effect of the CDW overcomes the positive one of biochar. As to the final amount of absorbed water, a qualitative correlation with the values reported in Figure 4 can be underlined. Moreover, the chemical characteristics of biochar make the modified samples less subject to efflorescence formation. This observation is, at present, only qualitative and not quantitative, thus requiring further experiments.

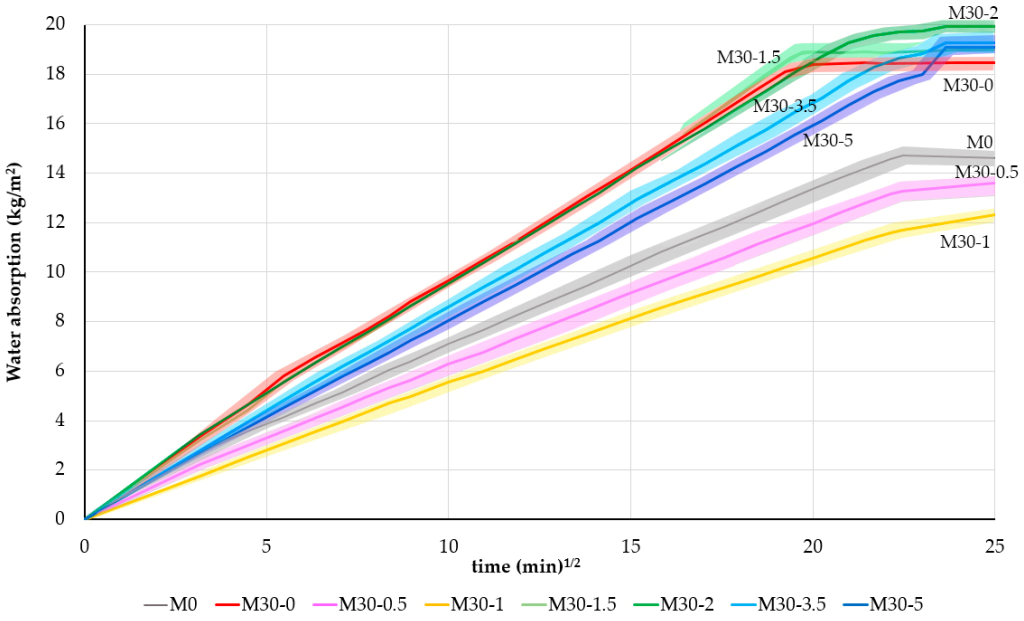


Figure 10. Water absorption by capillary curves (measurement variability included).

The curves obtained after the length change determination test are reported in Figure 11. As can be observed, all the samples containing CDW (M30 series) disclose lower shrinkage values than M-0 (about half of the final value at 14 days). Higher values are reported for the unmodified M30-0 sample compared to all the biochar-modified compositions (from 0.20% to 0.15%). However, the effect of biochar (from 1 to 5 wt%) is almost independent of its amount, and the plots tend to overlap. Dimensional shrinkage in alkali-activated materials is an extremely complex process in which many factors play an active role. The positive effect of CDW could derive from the different products formed during the curing

reactions, as well as the presence of crystalline phases like calcium carbonate. These factors overcome the intrinsic higher porosity of CDW samples. The beneficial effect of biochar could derive from a buffer effect on water evaporation, balancing the effect of increasing porosity. A deeper investigation is, however, necessary to clarify these mechanisms.

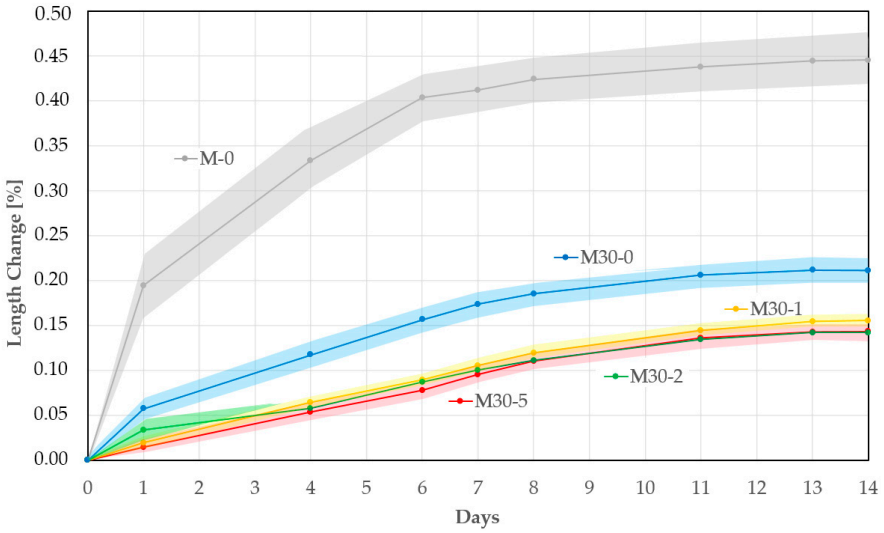


Figure 11. Length change determination curves (measurement variability included).

Small amounts of biochar (<1.5%) play an overall positive role in material performance. Mechanical properties are increased, allowing remarkable fractions of CDW to be introduced, without proceeding to a comprehensive but onerous characterization of the CDW and subsequent mix design of the components. This effect, which needs to be deeply investigated, can derive both from a nucleating impact and from a densification and reservoir role, as found in OPC mortars [37–39], or from the bridging capacity of biochar opposing crack propagation [40]. A densification effect in mortar with fly ash and ground granulated blast furnace slag was also observed by Wang [12] in samples incorporating pretreated biochar. However, a parameter that should be deeply investigated in the future is the possible active role of the organic fraction in the formation of alkali-activated products caused by the presence of specific functional groups [41]. Moreover, biochar is able to maintain a constant internal moisture content and alkalinity, and its organic aromatic feature hinders water permeation. Dimensional instability and water permeability are thus limited, and both these features can suggest improved durability, which needs to be further investigated by performing long-term dimensional stability measurements (>14 days), freeze–thaw cycles, and chloride and sulphate diffusion.

4. Conclusions

In this study, the replacement of biochar in metakaolin and CDW pastes (70% metakaolin, 15% brick waste and 15% concrete waste) is studied at different amounts of biochar (from 0.5 to 5%). The present conclusions refer to this specific mix design but may not hold for different materials. Concerning fresh-state properties, workability has an inverse proportionality with the amount of biochar, since the latter mainly absorbs water from the pastes, creating a denser mixture. Among physical properties, water absorption and open porosity were quite similar in all the investigated materials (21.9–23.4% and 32.9–34.0% respectively for WA and OP), although an almost direct proportional increase was observed for both WA and OP at increasing biochar addition. The effect of biochar on mechanical properties was positive for a small percentage of replacement ($\leq$1%). In particular, an increase in the mechanical properties was observed for 1% of biochar (compressive strength

increased +20% after 7 and 14 days, +30% after 28 days). Nucleation and the reservoir effect of biochar can be proposed for CDW–metakaolin pastes as found in OPC materials, but necessitate further investigation. Small biochar amounts (≤1%) also reduced the rate of capillary water absorption and qualitatively the amount of the efflorescences formed during the permeability test, although no quantitative evaluation can presently be proposed. At all the investigated amounts, biochar also increased dimensional stability. Future investigations (such as freeze/thaw cycles or chloride penetration) need to be performed in order to analyze the possible enhanced degradation stability induced by biochar.

Author Contributions: Conceptualization, S.M. and A.S.; methodology, S.M. and A.S.; investigation, S.M., L.B. and A.S.; writing—original draft preparation, L.B.; writing—review and editing, S.M. and A.S.; supervision, S.M. and A.S. All authors have read and agreed to the published version of the manuscript.

Funding: The authors acknowledge financial support from PRIN 2020-Secor PE8, project code 2020WEFKX5-004.

Data Availability Statement: The authors declare the availability of all the data reported in this paper.

Acknowledgments: The authors gratefully acknowledge A. Sgaravatto and A. Camanzi for technical support.

Conflicts of Interest: The authors declare no conflicts of interest.

References

1. Akinyemi, B.A.; Adesina, A. Recent advancements in the use of biochar for cementitious applications: A review. *J. Build. Eng.* **2020**, *32*, 101705. [CrossRef]
2. Amalina, F.; Razak, A.S.A.; Krishnan, S.; Sulaiman, H.; Zularisam, A.W.; Nasrullah, M. Advanced techniques in the production of biochar from lignocellulosic biomass and environmental applications. *Clean. Mater.* **2022**, *6*, 100137. [CrossRef]
3. Tayyab, S.; Ferdous, W.; Lokuge, W.; Siddique, R.; Manalo, A. Biochar in cementitious composites: A comprehensive review of properties, compatibility, and prospect of use in sustainable geopolymer concrete. *Res. Conserv. Recy. Adv.* **2025**, *25*, 200242. [CrossRef]
4. Danish, M.; Ahmad, T. A review on utilization of wood biomass as a sustainable precursor for activated carbon production and application. *Renew. Sustain. Energy Rev.* **2018**, *87*, 1–21. [CrossRef]
5. Chen, T.; Zhao, L.; Gao, X.; Li, L.; Qin, L. Modification of carbonation-cured cement mortar using biochar and its environmental evaluation. *Cem. Concr. Comp.* **2022**, *134*, 104764. [CrossRef]
6. Wang, L.; Chen, L.; Tsang, D.C.W.; Guo, B.; Yang, J.; Shen, Z.; Hou, D.; Ok, Y.S.; Poon, C.S. Biochar as green additives in cement-based composites with carbon dioxide curing. *J. Clean. Prod.* **2020**, *258*, 120678. [CrossRef]
7. Qing, L.; Zhang, H.; Zhang, Z. Effect of biochar on compressive strength and fracture performance of concrete. *J. Build. Eng.* **2023**, *78*, 107587. [CrossRef]
8. Suarez-Riera, D.; Falliano, D.; Ferro, G.A.; Tulliani, J.M.; Carvajal, J.F.; Bravo Celi, A.C.; Lavagna, L.; Restuccia, L. The effect of different biochar on the mechanical properties of cement-pastes and mortars. *Buildings* **2023**, *13*, 2900. [CrossRef]
9. Du, J.; Wang, Y.; Bao, Y.; Sarkar, D.; Meng, W. Valorization of wasted-derived biochar in ultra-high-performance concrete (UHPC): Pretreatment, characterization, and environmental benefits. *Constr. Build. Mater.* **2023**, *409*, 133839. [CrossRef]
10. Gupta, S.; Kua, H.W.; Low, C.Y. Use of biochar as carbon sequestering additive in cement mortar. *Cem. Concr. Comp.* **2018**, *87*, 110–129. [CrossRef]
11. Ciutac (Nicolaev), E.; Ghisman, V.; Iticescu, C.; Tcaciuc, D.; Buruiana, D.L. Industrial Waste Recycling for Sustainable Building Materials: A Review. *Buildings* **2026**, *16*, 1741. [CrossRef]
12. Wang, Y.; Takasu, K.; Zhao, Q.; Harada, K.; Liu, Z.; Suyama, H. Performance optimization and carbon reduction potential of bamboo biochar fine aggregates for sustainable geopolymer mortars. *Constr. Build. Mater.* **2025**, *497*, 143905. [CrossRef]
13. Prabahar, J.; Vafaei, B.; Baffoe, E.; Ghahremaininezhad, A. The effect of biochar on the properties of alkali-activated slag pastes. *Constr. Mater.* **2022**, *2*, 1–14. [CrossRef]
14. Zhu, X.; Zhang, Y.; Xu, W.; Ma, B.; Li, J.; Wang, L.; Yan, J.; Tsang, D.C.W. Microstructural and pore network evolution of biochar-modified alkali-activated slag cement. *J. Build. Eng.* **2025**, *115*, 114584. [CrossRef]
15. Noh, G.; Wu, X.; Jang, J.G. Effect of sequential acid-alkali biochar pretreatment on microstructure and strength of fly ash geopolymer mortars. *Constr. Build. Mater.* **2026**, *521*, 146120. [CrossRef]
16. Saccani, A.; Baldazzi, L.; Manzi, S. Effects of Biochar Addition on the properties of alkali-activated materials. *Materials* **2025**, *18*, 486. [CrossRef] [PubMed]

17. Alsharari, F. Utilization of industrial, agricultural, and construction waste in cementitious composites: A comprehensive review of their impact on concrete properties and sustainable construction practices. *Mater. Today Sust.* **2025**, *29*, 101080. [CrossRef]
18. Zhang, H.; Zhang, C.; He, B.; Yi, S.; Tang, L. Recycling fine powder collected from construction and demolition wastes as partial alternatives to cement: A comprehensive analysis on effects, mechanism, cost and CO_2 emission. *J. Build. Eng.* **2023**, *71*, 106507. [CrossRef]
19. Robayo-Salazar, R.A.; Rivera, J.F.; de Gutiérrez, R.M. Alkali-activated building materials made with recycled construction and demolition wastes. *Constr. Build. Mater.* **2017**, *149*, 130–138. [CrossRef]
20. Hwang, C.L.; Yehualaw, M.D.; Vo, D.H.; Huynh, T.P. Development of high-strength alkali-activated pastes containing high volumes of waste brick and ceramic powders. *Constr. Build. Mater.* **2019**, *218*, 519–529. [CrossRef]
21. Cardoza, A.; Colorado, H.A. Alkali activated manufactured by the alkaline activation of CDW using brick and concrete wastes. *Open Cer.* **2023**, *16*, 100438. [CrossRef]
22. Velardo, P.; Sáez del Bosque, I.F.; Sánchez de Rojas, M.I.; De Belie, N.; Medina, C. Design and evaluation of physical, mechanical and micro-structural properties of eco-friendly binary-blended mortars using biomass bottom ash or construction and demolition waste powder. *Cem. Concr. Comp.* **2023**, *143*, 105252. [CrossRef]
23. Baldazzi, L.; Saccani, A.; Manzi, S. Alkali-Activated Materials and CDW for the Development of Sustainable Building Materials: A Review with a Special Focus on Their Mechanical Properties. *Buildings* **2026**, *16*, 309. [CrossRef]
24. Manzi, S.; Mazzotti, C.; Bignozzi, M.C. Self-compacting concrete with recycled aggregate: Study of the long-term properties. *Constr. Build. Mater.* **2017**, *157*, 582–590. [CrossRef]
25. Manzi, S.; Baldazzi, L.; Saccani, A. Formulating geopolymer mortars through construction and demolition waste (CDW) recycling: A comprehensive case study. *Materials* **2023**, *16*, 7304. [CrossRef] [PubMed]
26. Sorrenti, G.; Masiello, C.A.; Dugan, B.; Toselli, M. Biochar physico-chemical properties as affected by environmental exposure. *Sci. Total Environ.* **2016**, *563–564*, 237–246. [CrossRef] [PubMed]
27. Javed, I.; Saeed, H.; Ekinci, A. Transforming Construction Waste into High-Performance Alkali-Activated Paste with Microstructural and Predictive π Modelling Insights. *Buildings* **2025**, *15*, 3830. [CrossRef]
28. *EN 772-13*; Determination of Net and Gross Dry Density. European Committee for Standardization: Brussels, Belgium, 2002.
29. *EN 772-21*; Determination of Water Absorption. European Committee for Standardization: Brussels, Belgium, 2011.
30. *EN 15801*; Conservation of Cultural Property-Test Methods-Determination of Water Absorption by Capillarity. European Committee for Standardization: Brussels, Belgium, 2010.
31. *EN 12504-4*; Testing Concrete in Structures—Part 4: Determination of Ultrasonic Pulse Velocity. European Committee for Standardization: Brussels, Belgium, 2021.
32. Yan, D.; Chen, S.; Zeng, Q.; Xu, S.; Li, H. Correlating the elastic properties of metakaolin-based geopolymer with its composition. *Mater. Des.* **2016**, *95*, 306–318. [CrossRef]
33. ASTM C 490/C 490M-21; Standard Practice for Use of Apparatus for the Determination of Length Change of Hardened Cement Paste, Mortar, and Concrete. ASTM International: West Conshohocken, PA, USA, 2021.
34. Wichmann, I.; Stephan, D. Phase formation and carbonation impact on the strength of alkali-activated demolition waste with calcium compounds. *Case Stud. Constr. Mater.* **2024**, *20*, e03312. [CrossRef]
35. Wang, H.; Wang, L.; Shen, W.; Cao, K.; Sun, L.; Wang, P.; Cui, L. Compressive strength, hydration and pore structure of alkali-activated slag mortars integrating with recycled concrete powder as binders. *KSCE J. Civ. Eng.* **2022**, *26*, 795–805. [CrossRef]
36. Ozcelikci, E.; Kul, A.; Gunal, M.F.; Ozel, B.F.; Yildirim, G.; Ashour, A.; Sahmaran, M. A comprehensive study on the compressive strength, durability-related parameters and microstructure of geopolymer mortars based on mixed construction and demolition waste. *J. Clean. Prod.* **2023**, *396*, 136522. [CrossRef]
37. Gupta, S.; Kua, H.W.; Pang, S.D. Biochar-mortar composite: Manufacturing, evaluation of physical properties and economic viability. *Constr. Build. Mater.* **2018**, *167*, 874–889. [CrossRef]
38. Gupta, S.; Kua, H.W. Carbonaceous micro-filler for cement: Effect of particle size and dosage of biochar on fresh and hardened properties of cement mortar. *Sci. Total Environ.* **2019**, *662*, 952–962. [CrossRef] [PubMed]
39. Gupta, S.; Muthukrishnan, S.; Kua, H.W. Comparing influence of inert biochar and silica rich biochar on cement mortar—Hydration kinetics and durability under chloride and sulfate environment. *Constr. Build. Mater.* **2021**, *268*, 121142. [CrossRef]
40. Shahmansouri, A.A.; Zhang, Z.; Jafari, H.A.; Shi, X. Biochar-amended high-strength engineered cementitious composites. *Cem. Concr. Comp.* **2025**, *164*, 10621. [CrossRef]
41. Catauro, M.; Papale, F.; Lamanna, G.; Bollino, F. Geopolymer/PEG hybrid materials synthesis and investigation of the polymer influence on microstructure and mechanical behavior. *Mater. Res.* **2015**, *18*, 698–705. [CrossRef]

Disclaimer/Publisher's Note: The statements, opinions and data contained in all publications are solely those of the individual author(s) and contributor(s) and not of MDPI and/or the editor(s). MDPI and/or the editor(s) disclaim responsibility for any injury to people or property resulting from any ideas, methods, instructions or products referred to in the content.